Sistemas Hidrotermais e Metalogênese

GSA 0407

MINERALIZAÇÕES DO TIPO PÓRFIRO

Caetano Juliani
(cjuliani@usp.br)
Lena Virgínia Soares Monteiro
(lena.monteiro@usp.br)

Departamento de Geologia Sedimentar e Ambiental
2019

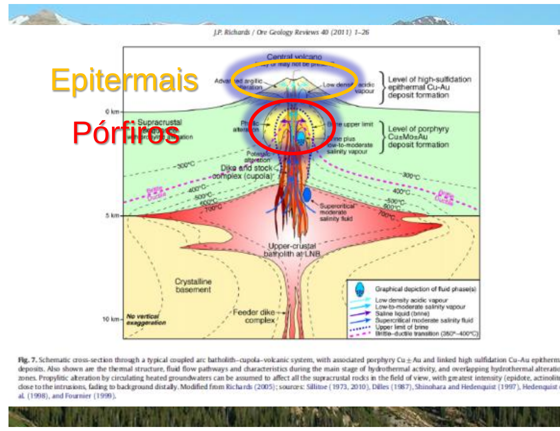

Fig. 7. Schematic cross-section through a typical coupled arc batholith–cupola–volcanic system, with associated porphyry Cu ± Au and linked high sulfidation Cu–Au epithermal deposits. Also shown are the thermal structure, fluid flow pathways and characteristics during the main stage of hydrothermal activity, and overlapping hydrothermal alteration zones. Propylitic alteration by circulating heated groundwaters can be assumed to affect all the supracrustal rocks in the field of view, with greatest intensity (epidote, actinolite) close to the intrusions, fading to background distally. Modified from Richards (2005); sources: Sillitoe (1973, 2010), Dilles (1987), Shinohara and Hedenquist (1997), Hedenquist et al. (1998), and Fournier (1999).

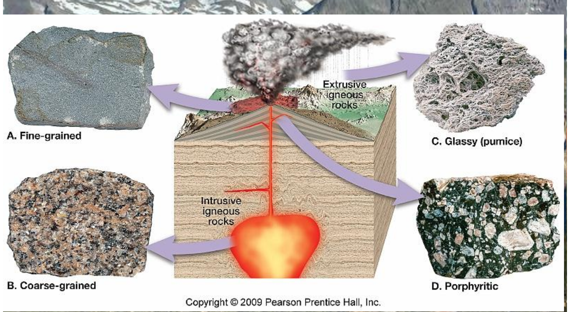

A Importância dos Pórfiros para os Recursos de Cobre e Ouro

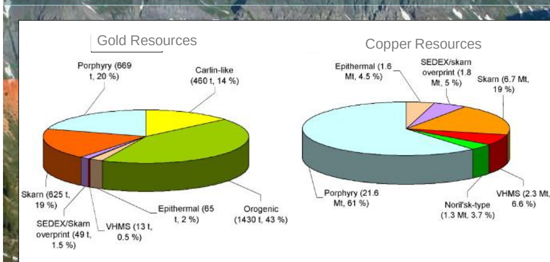

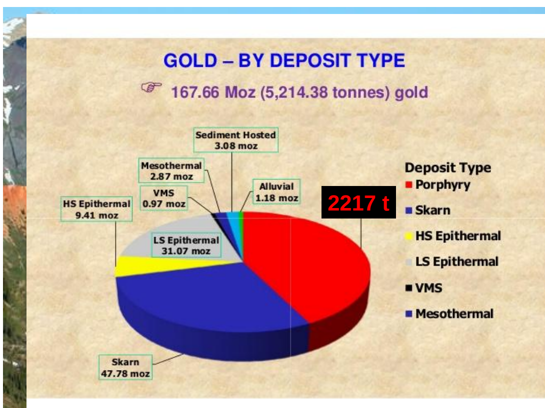

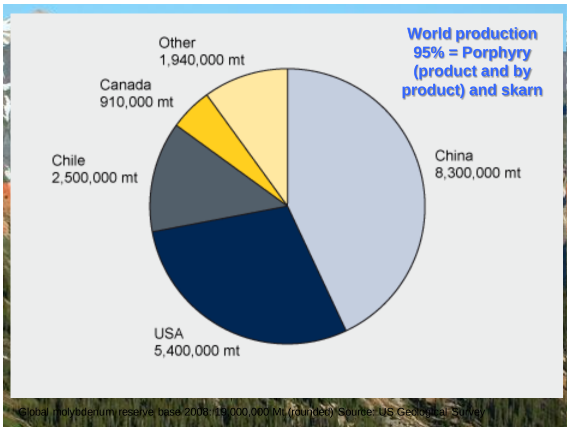
World production
95% = Porphyry
(product and by
product) and skarn
Other
1,940,000 mt
Canada
910,000 mt
Chile
2,500,000 mt
China
8,300,000 mt
USA
5,400,000 mt
Global molybdenum reserve base 2008: 19,000,000 Mt (rounded) Source: US Geological Survey

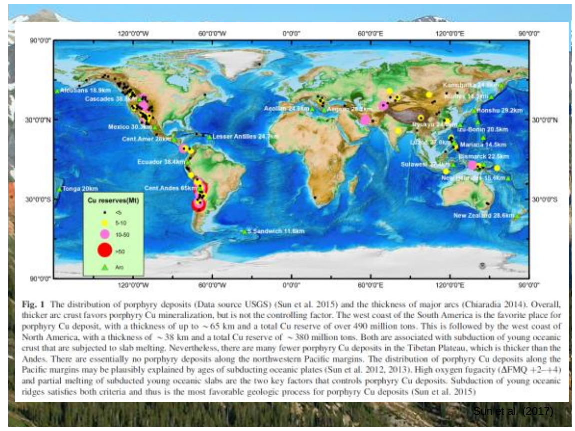
Cu reserves(Mt)
Fig. 1 The distribution of porphyry deposits (Data source USGS) (Sun et al. 2015) and the thickness of major arcs (Chiaradia 2014). Overall, thicker arc crust favors porphyry Cu mineralization, but is not the controlling factor. The west coast of the South America is the favorite place for porphyry Cu deposit, with a thickness of up to ~65 km and a total Cu reserve of over 490 million tons. This is followed by the west coast of North America, with a thickness of ~38 km and a total Cu reserve of ~380 million tons. Both are associated with subduction of young oceanic crust that are subjected to slab melting. Nevertheless, there are many fewer porphyry Cu deposits in the Tibetan Plateau, which is thicker than the Andes. There are essentially no porphyry deposits along the northwestern Pacific margins. The distribution of porphyry Cu deposits along the Pacific margins may be plausibly explained by ages of subducting oceanic plates (Sun et al. 2012, 2013). High oxygen fugacity (ΔFMQ +2–+4) and partial melting of subducted young oceanic slabs are the two key factors that controls porphyry Cu deposits. Subduction of young oceanic ridges satisfies both criteria and thus is the most favorable geologic process for porphyry Cu deposits (Sun et al. 2015)
Sun et al. (2017)

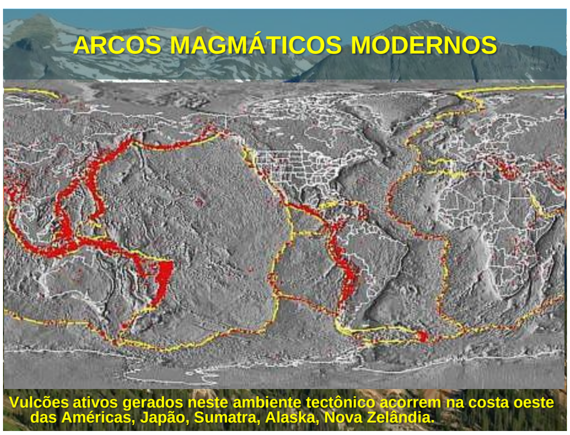
ARCOS MAGMÁTICOS MODERNOS
Vulcões ativos gerados neste ambiente tectônico ocorrem na costa oeste das Américas, Japão, Sumatra, Alaska, Nova Zelândia.

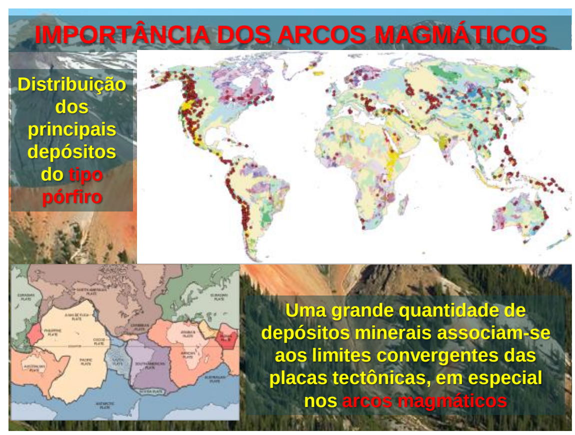
IMPORTÂNCIA DOS ARCOS MAGMÁTICOS
Distribuição dos principais depósitos do tipo pórfiro
Uma grande quantidade de depósitos minerais associam-se aos limites convergentes das placas tectônicas, em especial nos arcos magmáticos

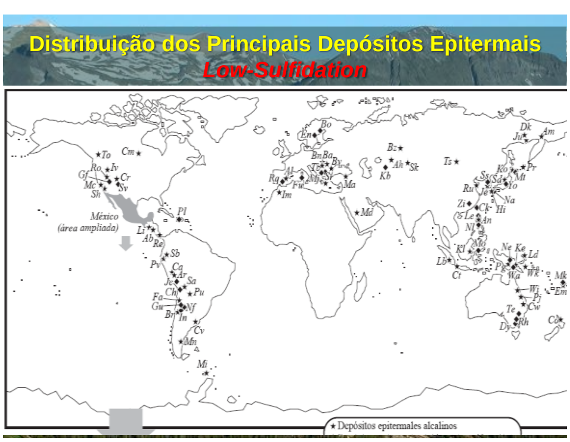
Distribuição dos Principais Depósitos Epitermais
Low-Sulfidation
México
(área ampliada)
★ Depósitos epitermales alcalinos

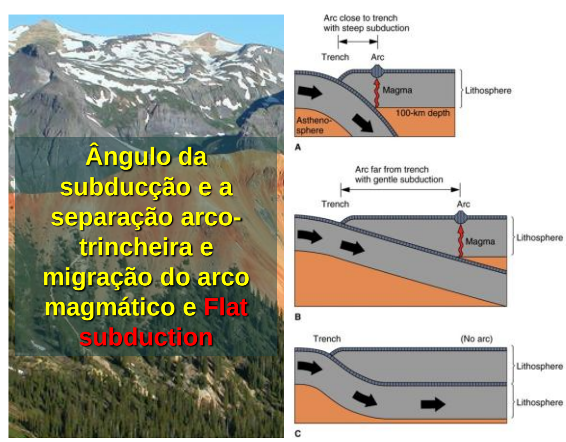
Ângulo da subducção e a separação arco-trincheira e migração do arco magmático e Flat subduction
Arc close to trench
with steep subduction
Trench
Arc
Magma
Lithosphere
Astheno-sphere
100-km depth
A
Arc far from trench
with gentle subduction
Trench
Arc
Magma
Lithosphere
B
Trench
(No arc)
Lithosphere
Lithosphere
C

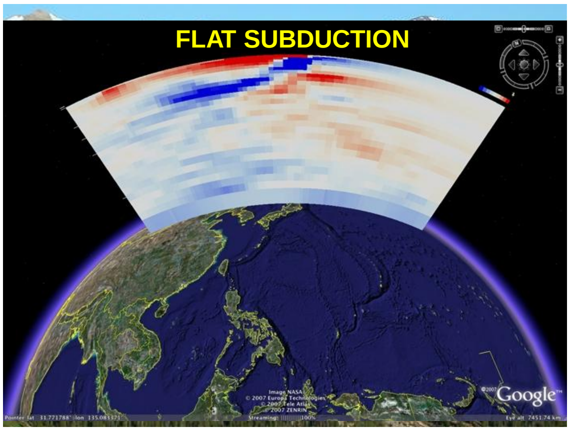
FLAT SUBDUCTION
Google

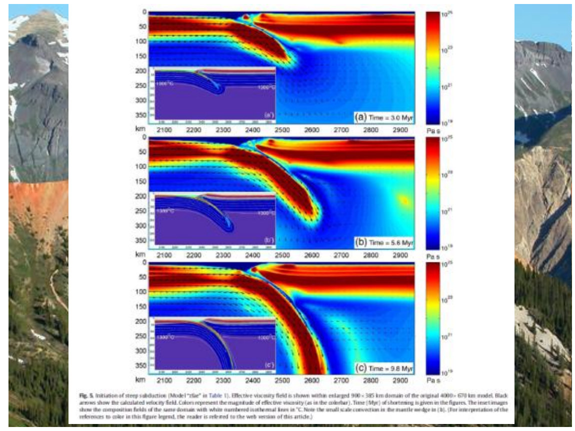
(a) Time = 3.0 Myr
(b) Time = 5.6 Myr
(c) Time = 9.8 Myr
Pa s
Fig. 5. Initiation of steep subduction (Model "zfae" in Table 1). Effective viscosity field is shown within enlarged 900 × 385 km domain of the original 4000 × 670 km model. Black arrows show the calculated velocity field. Colors represent the magnitude of effective viscosity (as in the colorbar). Time (Myr) of shortening is given in the figures. The inset images show the composition fields of the same domain with white numbered isothermal lines in °C. Note the small scale convection in the mantle wedge in (b). (For interpretation of the references to color in this figure legend, the reader is referred to the web version of this article.)

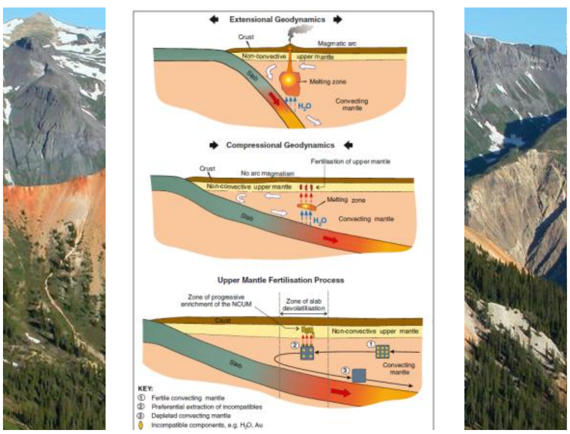
Extensional Geodynamics
Crust
Magmatic arc
Non-convective upper mantle
Melting zone
Slab
Convecting mantle
Compressional Geodynamics
Fertilisation of upper mantle
No arc magmatism
Non-convective upper mantle
Melting zone
Convecting mantle
Upper Mantle Fertilisation Process
Zone of progressive enrichment of the NCUM
Zone of slab devolatilisation
Non-convective upper mantle
Convecting mantle
KEY:
Fertile convecting mantle
Preferential extraction of incompatibles
Depleted convecting mantle
Incompatible components, e.g. H_2O, Au

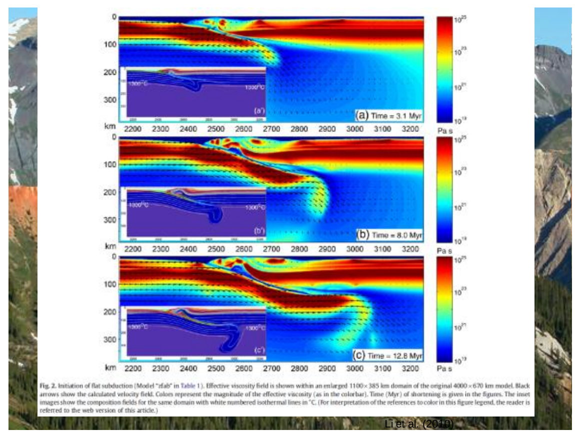
(a) Time = 3.1 Myr
(b) Time = 8.0 Myr
(c) Time = 12.8 Myr
Pa s
Fig. 2. Initiation of flat subduction (Model "zfab" in Table 1). Effective viscosity field is shown within an enlarged 1100 × 385 km domain of the original 4000 × 670 km model. Black arrows show the calculated velocity field. Colors represent the magnitude of the effective viscosity (as in the colorbar). Time (Myr) of shortening is given in the figures. The inset images show the composition fields for the same domain with white numbered isothermal lines in °C. (For interpretation of the references to color in this figure legend, the reader is referred to the web version of this article.)
Li et al. (2010)

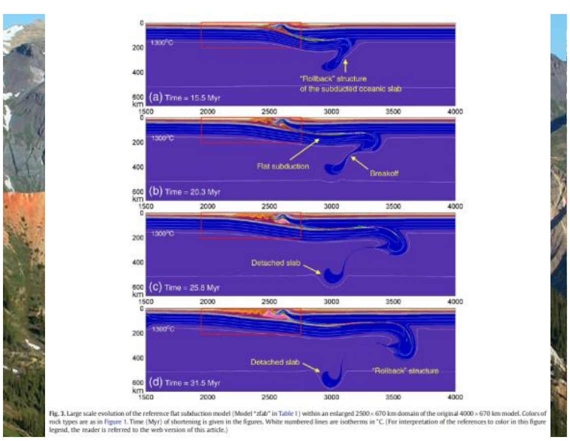
"Rollback" structure of the subducted oceanic slab
(a) Time = 15.5 Myr
Flat subduction
Breakoff
(b) Time = 20.3 Myr
Detached slab
(c) Time = 25.8 Myr
Detached slab
"Rollback" structure
(d) Time = 31.5 Myr
Fig. 3. Large scale evolution of the reference flat subduction model (Model "zfab" in Table 1) within an enlarged 2500 × 670 km domain of the original 4000 × 670 km model. Colors of rock types are as in Figure 1. Time (Myr) of shortening is given in the figures. White numbered lines are isotherms in °C. (For interpretation of the references to color in this figure legend, the reader is referred to the web version of this article.)

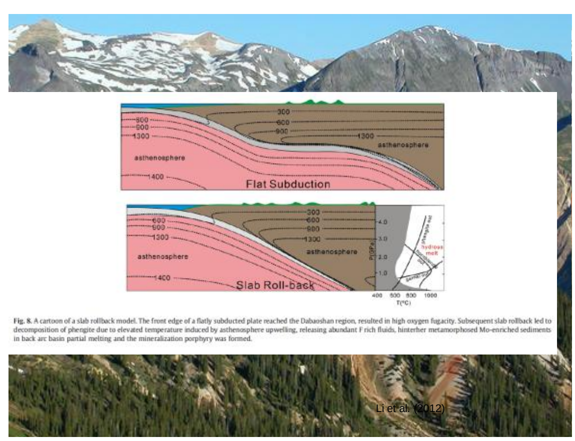
asthenosphere
Flat Subduction
asthenosphere
Slab Roll-back
hydrous melt
T(°C)
Fig. 8. A cartoon of a slab rollback model. The front edge of a flatly subducted plate reached the Dabaoshan region, resulted in high oxygen fugacity. Subsequent slab rollback led to decomposition of phengite due to elevated temperature induced by asthenosphere upwelling, releasing abundant F rich fluids, hinterher metamorphosed Mo-enriched sediments in back arc basin partial melting and the mineralization porphyry was formed.
Li et al. (2012)

CORDILHEIRA ANDINA

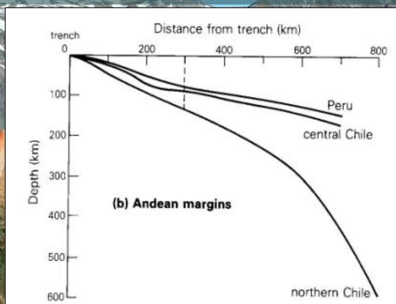

Na parte norte do Peru e na porção central do Chile o baixo ângulo de mergulho da placa subductante (<10º) não possibilita o vulcanismo ativo. Já no norte do Chile e no sul do Peru ângulo de subducção moderado do possibilita a geração d emagmas e o vulcanismo ativo.

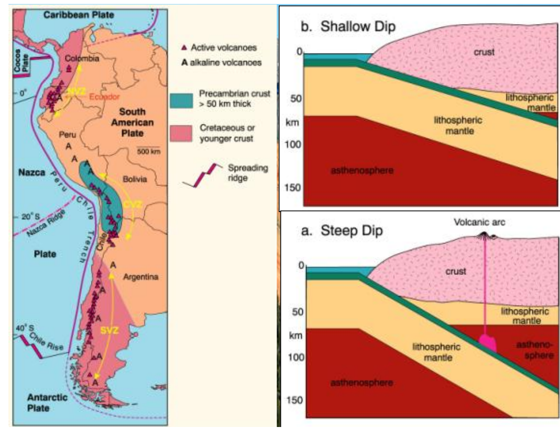

FLAT SUBDUCTION NO CHILE

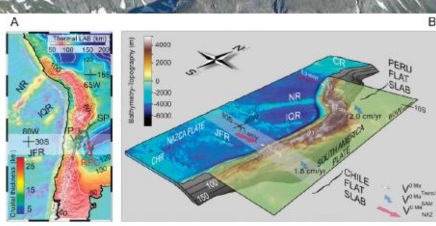

Figure 1. Relationship between observed data and subduction style along Andean subduction zone. A: Onshore: thermal lithosphere-asthenosphere boundary (LAB), defined as depth to 1300 °C (Tassara et al., 2006); flat subduction areas coincide with thick continental lithosphere. Red dashed line indicates western extent of Rio de la Plata craton (RPC), estimated to be ≥200 km thick from magnetotelluric studies (Booker et al., 2004; Favetto et al., 2008). SP—Sierras Pampeanas (dark gray), P—Precordillera (light gray). Offshore: oceanic crustal thickness derived from gravity modeling (Tassara et al., 2006). IQR—Iquique Ridge, JFR—Juan Fernandez Ridge, NR—Nazca Ridge. B: Three-dimensional view of Nazca and South American plates showing contours of depth in kilometers to Wadati-Benioff zone (Syracuse and Abers, 2006). Red, blue, and white arrows are present plate velocities (V) along the Peru-Chile Trench and of Nazca (NAZ) and South American (SAM) plates in Indo-Atlantic hotspot reference frame. East-west transparent bar shows modeled area. CR—Carnegie Ridge, CHR—Chile Ridge.

Manea et al. (2011)

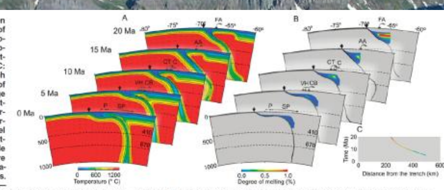

Figure 3. A: Evolution since Early Miocene of temperature field. B: Evolution since Early Miocene of degree of melting in mantle wedge. C: Distance from trench to surface projection of maximum mantle wedge melting for our best fitting model (Fig. 2B). During each time interval surface projection of model maximum degree of melting and highest mantle wedge temperature coincide well with locations of active volcanoes. FA—Farellones Arc, AA—Aconcagua, CT—Cerro de las Tortolas, C—Calingasta, VH—Vacas Heladas, CB—Cerro Blanco, P—Precordillera, SP—Sierras Pampeanas.

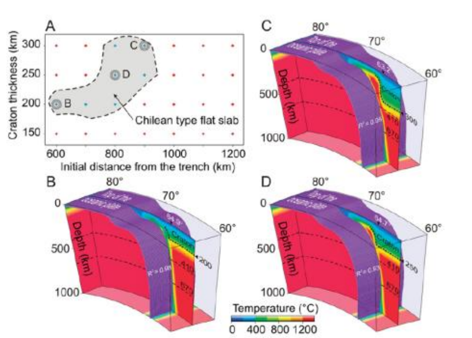

Figure 2. A: Domain diagram showing style of subduction as function of craton depth and initial distance from trench. Gray domain indicates models where slab geometry after 30 m.y. of evolution best fits present-day slab geometry and craton to trench distance (64°W ± 1°) in flat slab region of Chile. B, C, D: Temperature and geometry after 30 m.y. of evolution of three best-fitting models for flat slab domain in A. Dashed black lines represent craton shape; locations (in degrees; white lettering) of craton edge in each model are indicated.

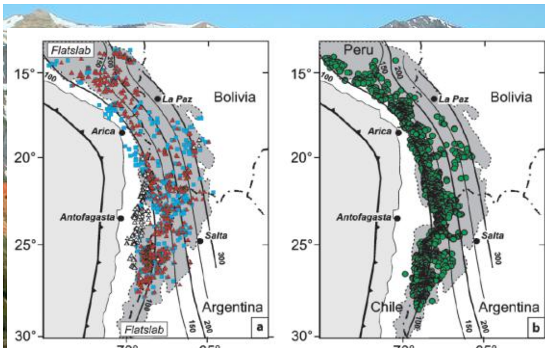

Trumbull *et al.* (2006)

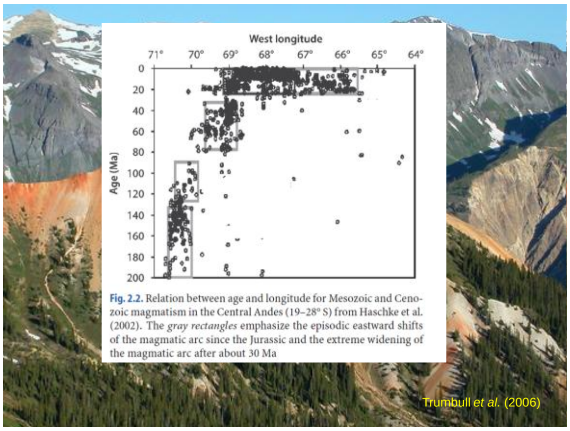
West longitude
Age (Ma)
Fig. 2.2. Relation between age and longitude for Mesozoic and Cenozoic magmatism in the Central Andes (19–28° S) from Haschke et al. (2002). The gray rectangles emphasize the episodic eastward shifts of the magmatic arc since the Jurassic and the extreme widening of the magmatic arc after about 30 Ma
Trumbull et al. (2006)

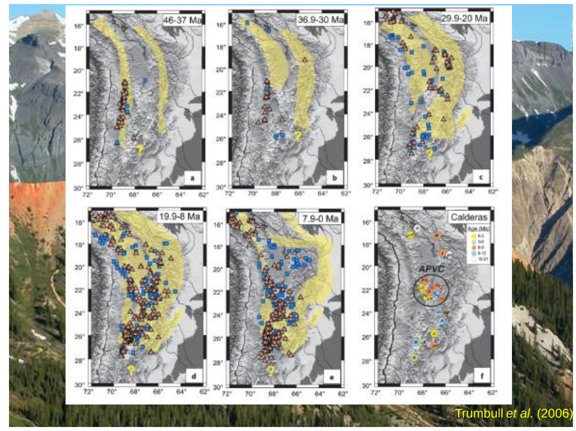
46-37 Ma
36.9-30 Ma
29.9-20 Ma
19.9-8 Ma
7.9-0 Ma
Calderas
APVC
Trumbull et al. (2006)

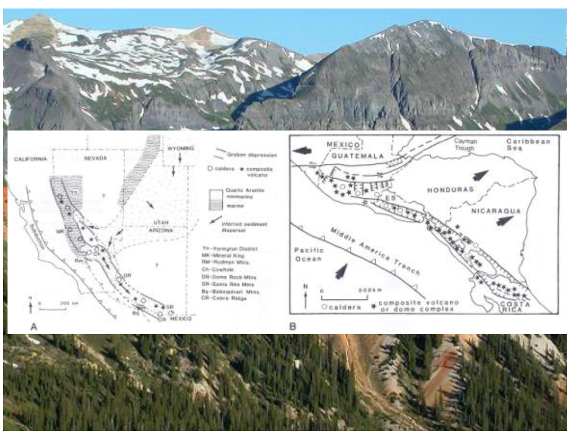
CALIFORNIA
NEVADA
WYOMING
UTAH
ARIZONA
MEXICO
GUATEMALA
HONDURAS
NICARAGUA
Caribbean Sea
Pacific Ocean
Middle America Trench
COSTA RICA
A
B

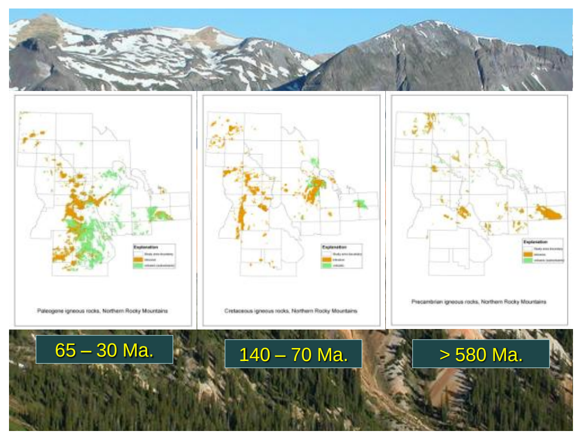
Paleogene igneous rocks, Northern Rocky Mountains
Cretaceous igneous rocks, Northern Rocky Mountains
Precambrian igneous rocks, Northern Rocky Mountains
65 – 30 Ma.
140 – 70 Ma.
> 580 Ma.

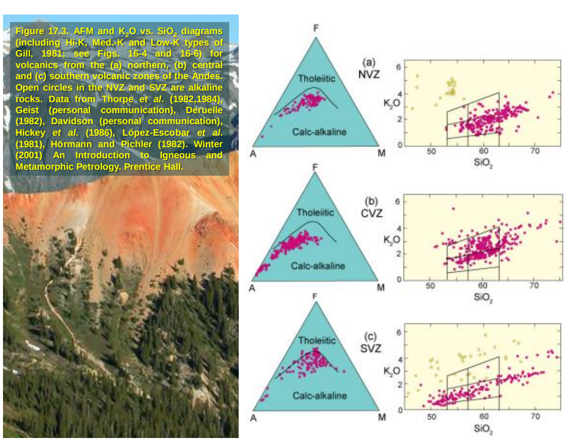
Figure 17.3. AFM and K_2O vs. SiO_2 diagrams (including Hi-K, Med.-K and Low-K types of Gill, 1981; see Figs. 16-4 and 16-6) for volcanics from the (a) northern, (b) central and (c) southern volcanic zones of the Andes. Open circles in the NVZ and SVZ are alkaline rocks. Data from Thorpe et al. (1982,1984), Geist (personal communication), Deruelle (1982), Davidson (personal communication), Hickey et al. (1986), López-Escobar et al. (1981), Hörmann and Pichler (1982). Winter (2001) An Introduction to Igneous and Metamorphic Petrology. Prentice Hall.
F
Tholeiitic
Calc-alkaline
A
M
(a) NVZ
(b) CVZ
(c) SVZ
K_2O
SiO_2

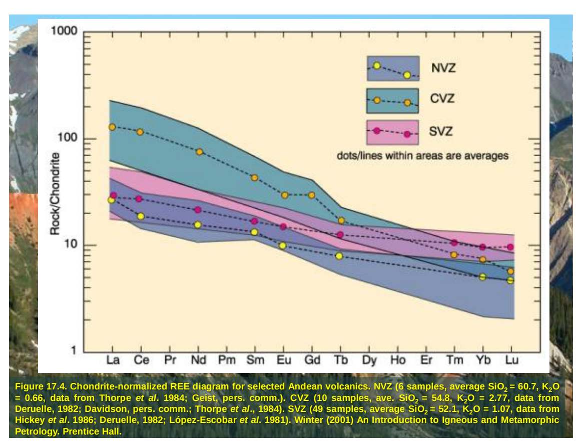
Rock/Chondrite
NVZ
CVZ
SVZ
dots/lines within areas are averages
La Ce Pr Nd Pm Sm Eu Gd Tb Dy Ho Er Tm Yb Lu
Figure 17.4. Chondrite-normalized REE diagram for selected Andean volcanics. NVZ (6 samples, average SiO_2 = 60.7, K_2O = 0.66, data from Thorpe et al. 1984; Geist, pers. comm.). CVZ (10 samples, ave. SiO_2 = 54.8, K_2O = 2.77, data from Deruelle, 1982; Davidson, pers. comm.; Thorpe et al., 1984). SVZ (49 samples, average SiO_2 = 52.1, K_2O = 1.07, data from Hickey et al. 1986; Deruelle, 1982; López-Escobar et al. 1981). Winter (2001) An Introduction to Igneous and Metamorphic Petrology. Prentice Hall.

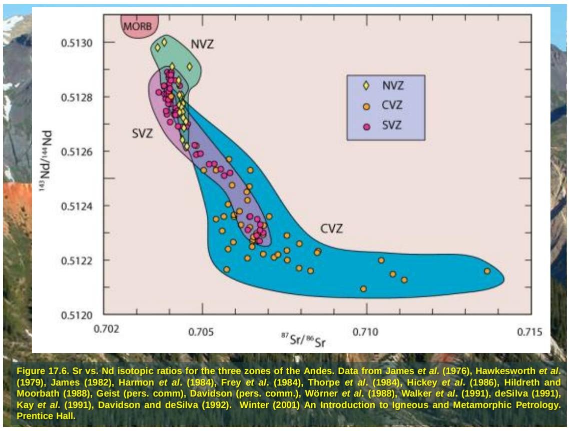

Figure 17.6. Sr vs. Nd isotopic ratios for the three zones of the Andes. Data from James *et al.* (1976), Hawkesworth *et al.* (1979), James (1982), Harmon *et al.* (1984), Frey *et al.* (1984), Thorpe *et al.* (1984), Hickey *et al.* (1986), Hildreth and Moorbath (1988), Geist (pers. comm), Davidson (pers. comm.), Wörner *et al.* (1988), Walker *et al.* (1991), deSilva (1991), Kay *et al.* (1991), Davidson and deSilva (1992). Winter (2001) An Introduction to Igneous and Metamorphic Petrology. Prentice Hall.

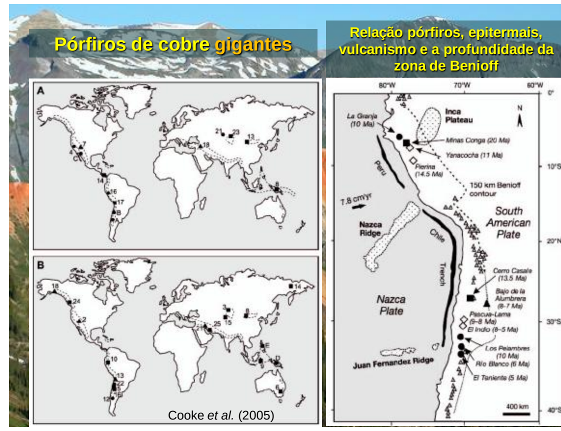

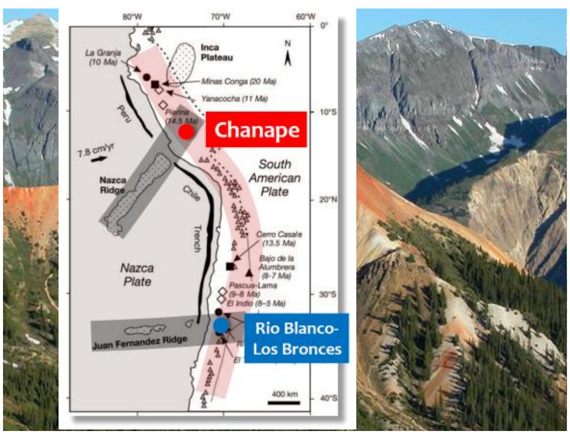

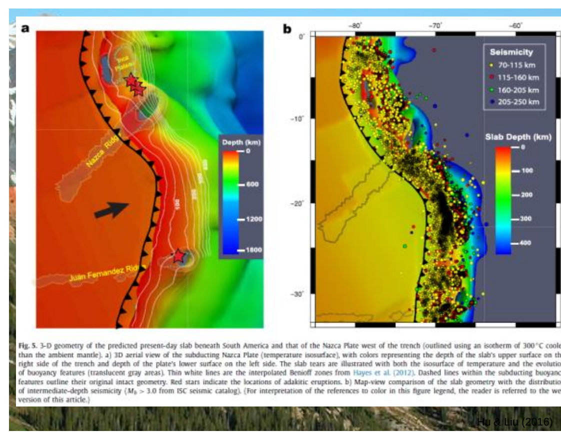

Fig. 5. 3-D geometry of the predicted present-day slab beneath South America and that of the Nazca Plate west of the trench (outlined using an isotherm of 300 °C cooler than the ambient mantle). a) 3D aerial view of the subducting Nazca Plate (temperature isosurface), with colors representing the depth of the slab's upper surface on the right side of the trench and depth of the plate's lower surface on the left side. The slab tears are illustrated with both the isosurface of temperature and the evolution of buoyancy features (translucent gray areas). Thin white lines are the interpolated Benioff zones from Hayes et al. (2012). Dashed lines within the subducting buoyancy features outline their original intact geometry. Red stars indicate the locations of adakitic eruptions. b) Map-view comparison of the slab geometry with the distribution of intermediate-depth seismicity ($M_b > 3.0$ from ISC seismic catalog). (For interpretation of the references to color in this figure legend, the reader is referred to the web version of this article.)

Hu & Liu (2016)

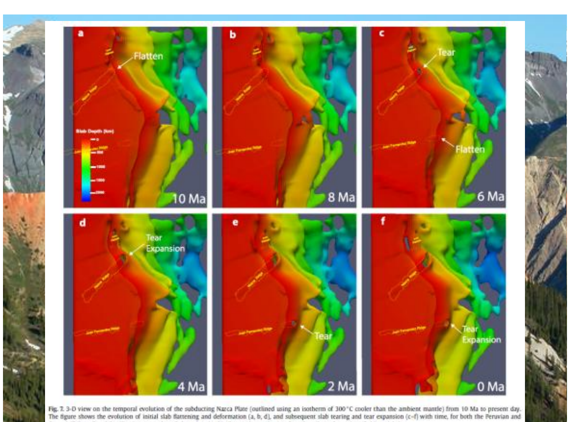

Fig. 7. 3-D view on the temporal evolution of the subducting Nazca Plate (outlined using an isotherm of 300 °C cooler than the ambient mantle) from 10 Ma to present day. The figure shows the evolution of initial slab flattening and deformation (a, b, d), and subsequent slab tearing and tear expansion (c–f) with time, for both the Peruvian and Central Chilean flat slabs. (For interpretation of the colors in this figure, the reader is referred to the web version of this article.)

Hu & Liu (2016)

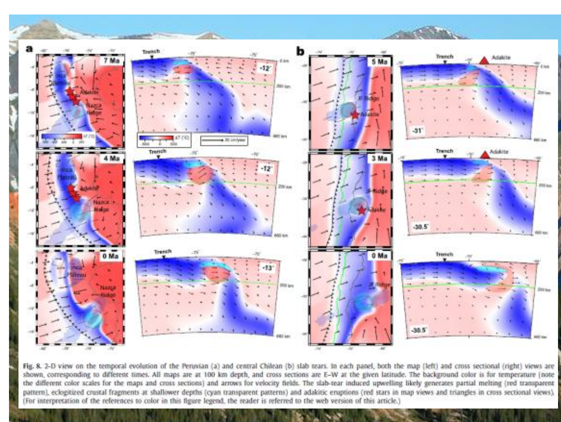

Fig. 8. 2-D view on the temporal evolution of the Peruvian (a) and central Chilean (b) slab tears. In each panel, both the map (left) and cross sectional (right) views are shown, corresponding to different times. All maps are at 100 km depth, and cross sections are E–W at the given latitude. The background color is for temperature (note the different color scales for the maps and cross sections) and arrows for velocity fields. The slab-tear induced upwelling likely generates partial melting (red transparent pattern), eclogitized crustal fragments at shallower depths (cyan transparent patterns) and adakitic eruptions (red stars in map views and triangles in cross sectional views). (For interpretation of the references to color in this figure legend, the reader is referred to the web version of this article.)

Hu & Liu (2016)

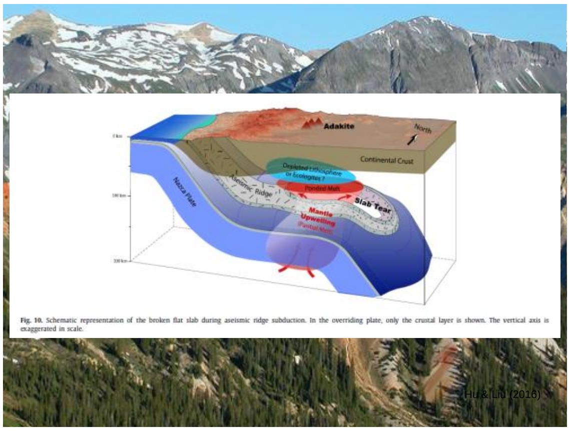
Adakite
North
Continental Crust
Nazca Plate
Ridge
Slab Tear
Mantle Upwelling
Fig. 10. Schematic representation of the broken flat slab during aseismic ridge subduction. In the overriding plate, only the crustal layer is shown. The vertical axis is exaggerated in scale.
Hu & Liu (2016)

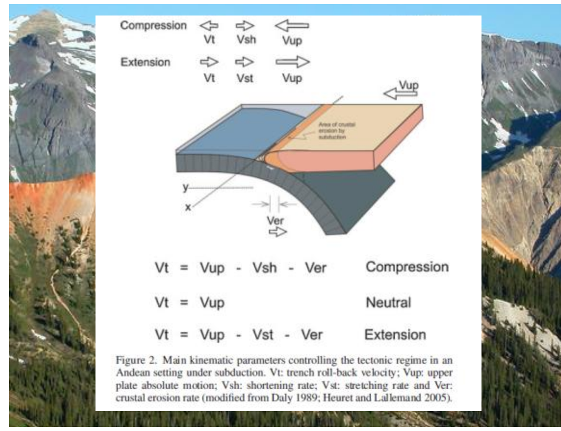
Compression Vt Vsh Vup
Extension Vt Vst Vup
Vup
y
x
Ver
Vt = Vup - Vsh - Ver Compression
Vt = Vup Neutral
Vt = Vup - Vst - Ver Extension
Figure 2. Main kinematic parameters controlling the tectonic regime in an Andean setting under subduction. Vt: trench roll-back velocity; Vup: upper plate absolute motion; Vsh: shortening rate; Vst: stretching rate and Ver: crustal erosion rate (modified from Daly 1989; Heuret and Lallemand 2005).

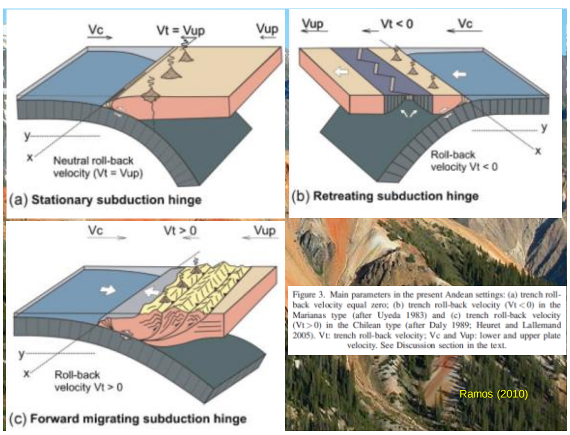
Vc Vt = Vup Vup
y
x
Neutral roll-back velocity (Vt = Vup)
(a) Stationary subduction hinge
Vup Vt < 0 Vc
y
x
Roll-back velocity Vt < 0
(b) Retreating subduction hinge
Vc Vt > 0 Vup
y
x
Roll-back velocity Vt > 0
(c) Forward migrating subduction hinge
Figure 3. Main parameters in the present Andean settings: (a) trench roll-back velocity equal zero; (b) trench roll-back velocity (Vt < 0) in the Marianas type (after Uyeda 1983) and (c) trench roll-back velocity (Vt > 0) in the Chilean type (after Daly 1989; Heuret and Lallemand 2005). Vt: trench roll-back velocity; Vc and Vup: lower and upper plate velocity. See Discussion section in the text.
Ramos (2010)

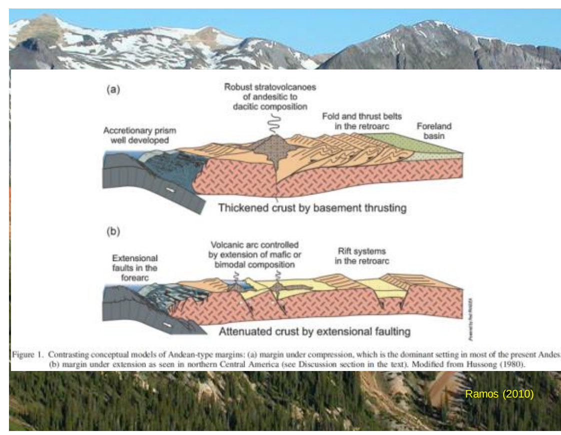
(a)
Robust stratovolcanoes of andesitic to dacitic composition
Accretionary prism well developed
Fold and thrust belts in the retroarc
Foreland basin
Thickened crust by basement thrusting
(b)
Extensional faults in the forearc
Volcanic arc controlled by extension of mafic or bimodal composition
Rift systems in the retroarc
Attenuated crust by extensional faulting
Figure 1. Contrasting conceptual models of Andean-type margins: (a) margin under compression, which is the dominant setting in most of the present Andes; (b) margin under extension as seen in northern Central America (see Discussion section in the text). Modified from Hussong (1980).
Ramos (2010)

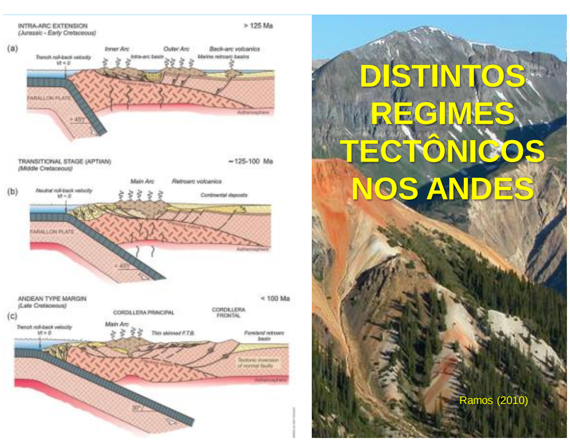
INTRA-ARC EXTENSION (Jurassic - Early Cretaceous) > 125 Ma
(a)
TRANSITIONAL STAGE (APTIAN) (Middle Cretaceous) ~125-100 Ma
(b)
ANDEAN TYPE MARGIN (Late Cretaceous) < 100 Ma
(c)
DISTINTOS REGIMES TECTÔNICOS NOS ANDES
Ramos (2010)

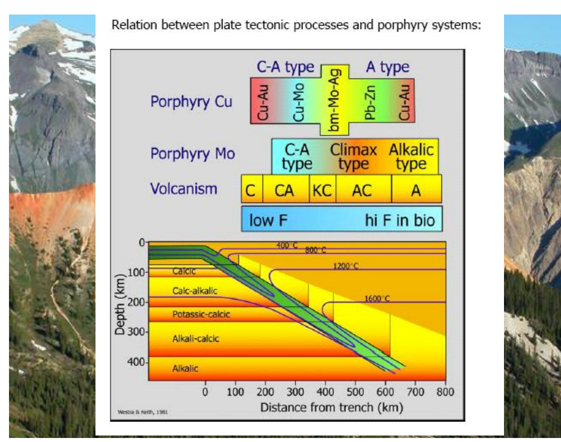
Relation between plate tectonic processes and porphyry systems:
C-A type
A type
Porphyry Cu
Cu-Au
Cu-Mo
bm-Mo-Ag
Pb-Zn
Cu-Au
Porphyry Mo
C-A type
Climax type
Alkalic type
Volcanism
C
CA
KC
AC
A
low F
hi F in bio
Depth (km)
Calcic
Calc-alkalic
Potassic-calcic
Alkali-calcic
Alkalic
400°C
800°C
1200°C
1600°C
Distance from trench (km)

GERAÇÃO DE MAGMAS

- A água é fornecida pelas reações metamórficas de desidratação na base de uma pilha sedimentar e na crosta oceânica hidratada no funco oceânico.
- A água liberada e calor favorecem a anatexia nas rochas da base da crosta continental, independentemente de sua natureza.

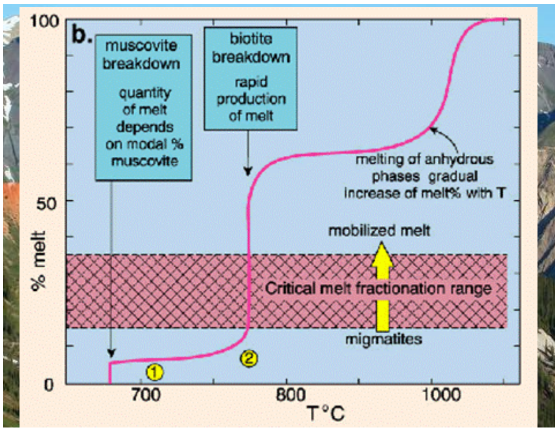

OS GRANITÓIDES

- O fato de que todos os sistemas magmáticos se fracionam em maior ou menor intensidade para uma associação de quartzo + feldspato fundido, o que faz com que os granitos constituam o produto do sistema residual petrogenético
- O sistema ternário demonstra que os magmas graníticos poderiam ser gerados tanto a partir de processos de diferenciação de magmas como a partir do fundido parcial de rochas (anatexia) da crosta continental quando se fundem os minerais de mínimo ponto de fusão.

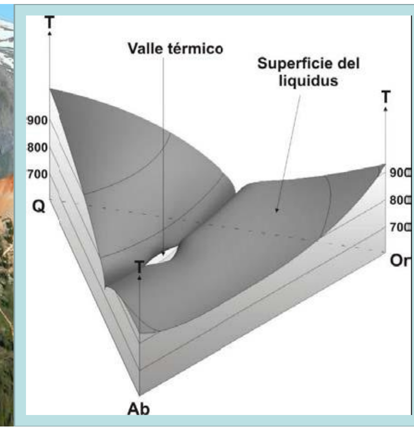

OS GRANITÓIDES

A fusão parcial das rochas (anatexia) é causada por:

- A descompressão adiabática de rochas sólidas a altas temperaturas
- Ingresso de água a sistema
- Aumento da temperatura.

FATORES QUE INFLUEM NA GERAÇÃO DE MAGMAS

- A água liberada por reações metamórficas na placa oceânica que mergulha sob continente cumpre duas funções: produzir a fusão parcial do manto peridotito na cunha astenosférica e promover um enriquecimento metasomático do manto pelo aporte de elementos solúveis. A menor densidade dos fluidos basálticos e andesiticos produzidos faz com que esses ascendam através do manto e se concentrem na base da crosta continental.
- A cristalização em profundidades de estes magmas produzem liberação da água dissolvida e do calor no entorno da intrusão, promovendo a fusão parcial da crosta.

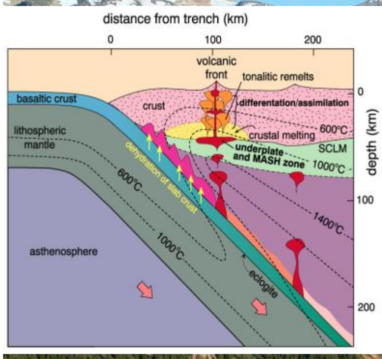

Secção esquemática de uma zona de subducção numa margem continental ativa onde se observa desidratação da placa oceânica que mergulha sob o continente, a hidratação e fusão da cunha de manto, a zona de *underplate*, onde se desenvolvem os processos de MASH (*Melting, Assimilation, Storage, Homogenization*) e os fenômenos de diferenciação que se desenvolvem na crosta.

ARCO MAGMÁTICO

- O tipo de magmatismo produzido no ambiente de margem ativa é bem mais complexo que o magmatismo do ambiente de arco de ilhas, devido à passagem do magma pela crosta continental que introduz várias complexidades (diferentes fontes, contaminação, assimilação, mistura de magmas, etc) para o processo

Porphyry deposits are (Kirkham, 1972):

1) Large, low- to medium-grade deposits in which primary (hypogene) ore minerals are dominantly
2) Structurally controlled deposits
3) Spatially and genetically related to felsic to intermediate porphyritic intrusions

.

The large size and structural control (e.g. veins, vein sets, stockworks, fractures, 'crackled zones', and breccias) serve to distinguish porphyry deposits from a variety of deposits that may be peripherally associated, including skarns, high-temperature mantos, peripheral mesothermal veins, and epithermal precious-metal deposits.

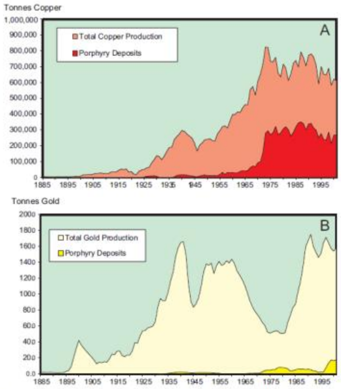

FIGURE 3. Canadian production of copper (A) and gold (B) between 1885 and 2000. Data are from Natural Resources Canada and Statistics Canada.

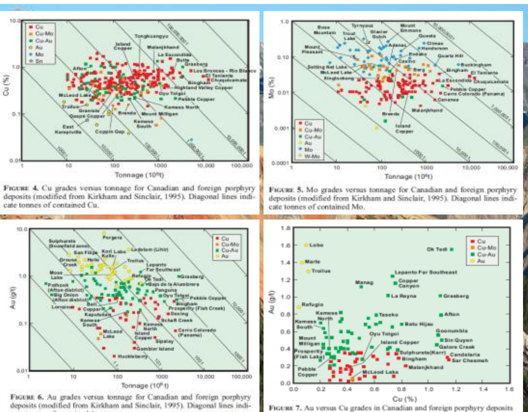

FIGURE 4. Cu grades versus tonnage for Canadian and foreign porphyry deposits (modified from Kirkham and Sinclair, 1995). Diagonal lines indicate tonnes of contained Cu.

FIGURE 5. Mo grades versus tonnage for Canadian and foreign porphyry deposits (modified from Kirkham and Sinclair, 1995). Diagonal lines indicate tonnes of contained Mo.

FIGURE 6. Au grades versus tonnage for Canadian and foreign porphyry deposits (modified from Kirkham and Sinclair, 1995). Diagonal lines indicate tonnes of contained Au.

FIGURE 7. Au versus Cu grades in Canadian and foreign porphyry deposits (modified from Kirkham and Sinclair, 1995).

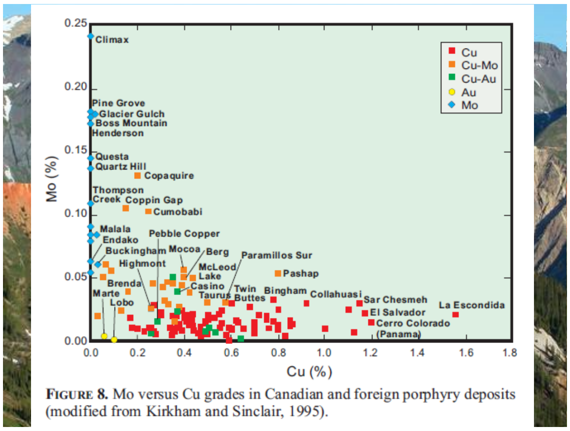

FIGURE 8. Mo versus Cu grades in Canadian and foreign porphyry deposits (modified from Kirkham and Sinclair, 1995).

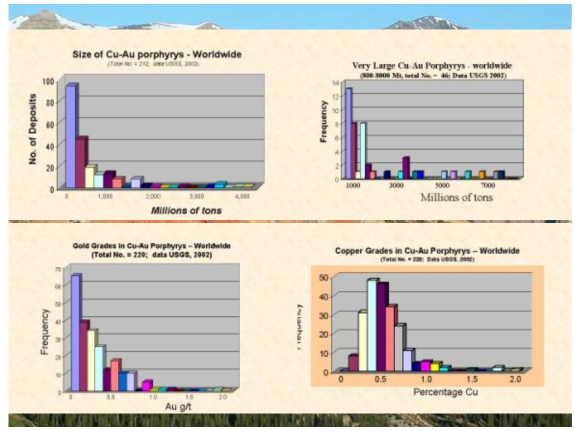

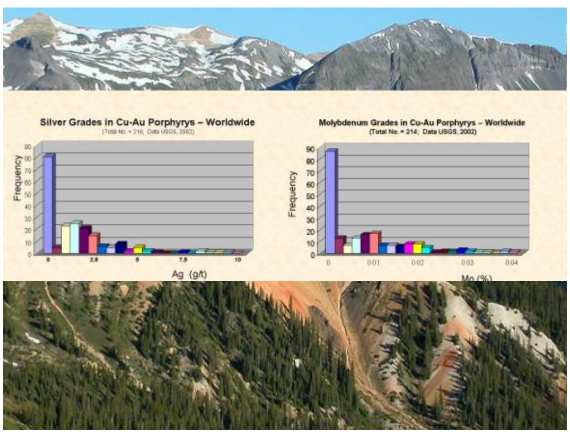

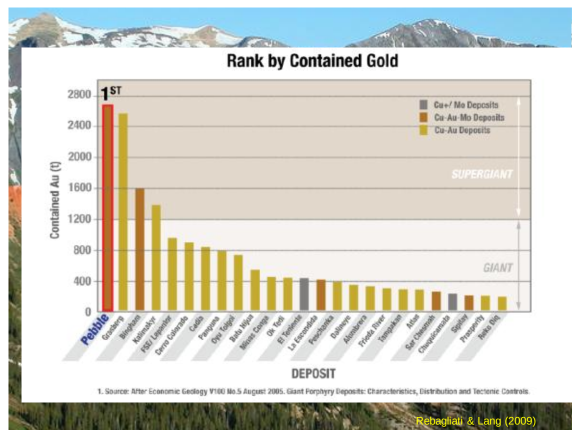

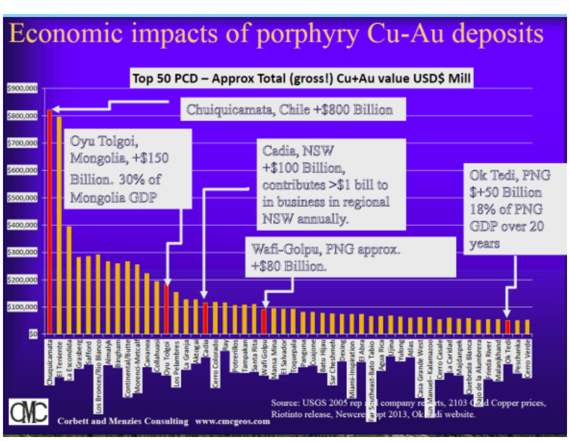

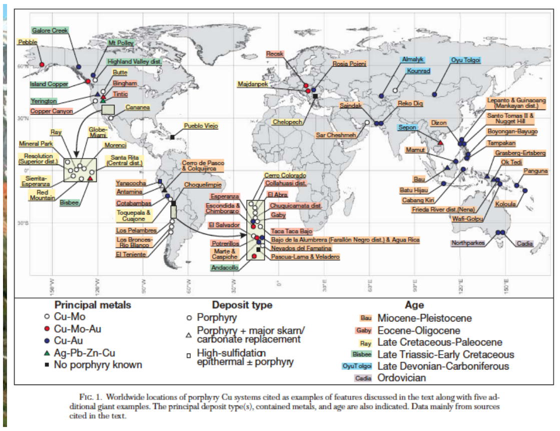

FIG. 1. Worldwide locations of porphyry Cu systems cited as examples of features discussed in the text along with five additional giant examples. The principal deposit type(s), contained metals, and age are also indicated. Data mainly from sources cited in the text.

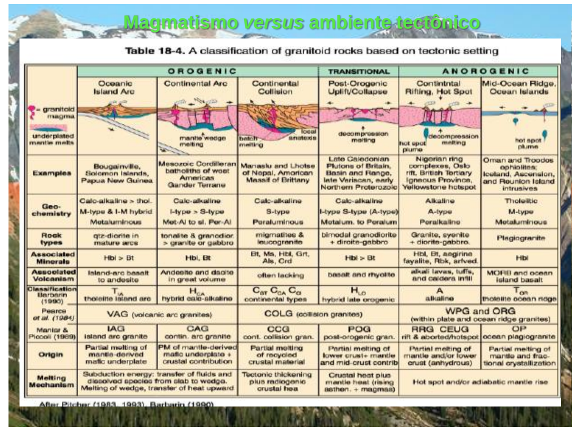

Table 18-4. A classification of granitoid rocks based on tectonic setting

	OROGENIC			TRANSITIONAL	ANOROGENIC	
	Oceanic Island Arc	Continental Arc	Continental Collision	Post-Orogenic Uplift/Collapse	Contintntal Rifting, Hot Spot	Mid-Ocean Ridge, Ocean Islands
granitoid magma; underplated mantle melts		mantle wedge melting	batch melting; local anatexis	decompression melting	hot spot plume; decompression melting	hot spot plume
Examples	Bougainville, Solomon Islands, Papua New Guinea	Mesozoic Cordilleran batholiths of west Americas Gander Terrane	Manaslu and Lhotse of Nepal, American Massif of Brittany	Late Caledonian Plutons of Britain, Basin and Range, late Variscan, early Northern Proterozoic	Nigerian ring complexes, Oslo rift, British Tertiary Igneous Province, Yellowstone hotspot	Oman and Troodos ophiolites; Iceland, Ascension, and Reunion Island intrusives
Geo-chemistry	Calc-alkaline > thol. M-type & I-M hybrid Metaluminous	Calc-alkaline I-type > S-type Met-Al to sl. Per-Al	Calc-alkaline S-type Peraluminous	Calc-alkaline I-type S-type (A-type) Metalum. to Peralum	Alkaline A-type Peralkaline	Tholeiitic M-type Metaluminous
Rock types	qtz-diorite in mature arcs	tonalite & granodior. > granite or gabbro	migmatites & leucogranite	bimodal granodiorite + diroite-gabbro	Granite, syenite + diorite-gabbro.	Plagiogranite
Associated Minerals	Hbl > Bt	Hbl, Bt	Bt, Ms, Hbl, Grt, Als, Crd	Hbl > Bt	Hbl, Bt, aegirine fayalite, Rbk, arfved.	Hbl
Associated Volcanism	Island-arc basalt to andesite	Andesite and dacite in great volume	often lacking	basalt and rhyolite	alkali lavas, tuffs, and caldera infill	MORB and ocean island basalt
Classification Barbarin (1990)	T_{IA} tholeiite island arc	H_{CA} hybrid calc-alkaline	C_{ST} C_{CA} C_{CI} continental types	H_{LO} hybrid late orogenic	A alkaline	T_{OR} tholeiite ocean ridge
Pearce et al. (1984)	VAG (volcanic arc granites)		COLG (collision granites)		WPG and ORG (within plate and ocean ridge granites)	
Maniar & Piccoli (1989)	IAG island arc granite	CAG contin. arc granite	CCG cont. collision gran.	POG post-orogenic gran.	RRG CEUG rift & aborted/hotspot	OP ocean plagiogranite
Origin	Partial melting of mantle-derived mafic underplate	PM of mantle-derived mafic underplate + crustal contribution	Partial melting of recycled crustal material	Partial melting of lower crust+ mantle and mid-crust contrib	Partial melting of mantle and/or lower crust (anhydrous)	Partial melting of mantle and fractional crystallization
Melting Mechanism	Subduction energy: transfer of fluids and dissolved species from slab to wedge. Melting of wedge, transfer of heat upward		Tectonic thickening plus radiogenic crustal hea	Crustal heat plus mantle heat (rising asthen. + magmas)	Hot spot and/or adiabatic mantle rise	

After Pitcher (1983, 1993), Barbarin (1990)

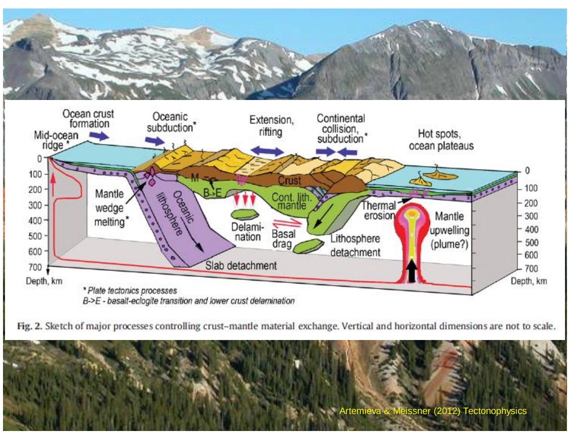

Fig. 2. Sketch of major processes controlling crust–mantle material exchange. Vertical and horizontal dimensions are not to scale.

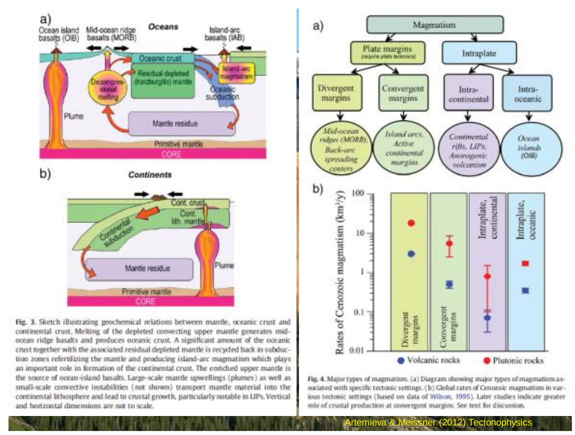

Fig. 3. Sketch illustrating geochemical relations between mantle, oceanic crust and continental crust. Melting of the depleted convecting upper mantle generates mid-ocean ridge basalts and produces oceanic crust. A significant amount of the oceanic crust together with the associated residual depleted mantle is recycled back in subduction zones refertilizing the mantle and producing island-arc magmatism which plays an important role in formation of the continental crust. The enriched upper mantle is the source of ocean-island basalts. Large-scale mantle upwellings (plumes) as well as small-scale convective instabilities (not shown) transport mantle material into the continental lithosphere and lead to crustal growth, particularly notable in LIPs. Vertical and horizontal dimensions are not to scale.

Fig. 4. Major types of magmatism. (a) Diagram showing major types of magmatism associated with specific tectonic settings. (b) Global rates of Cenozoic magmatism in various tectonic settings (based on data of Wilson, 1995). Later studies indicate greater role of crustal production at convergent margins. See text for discussion.

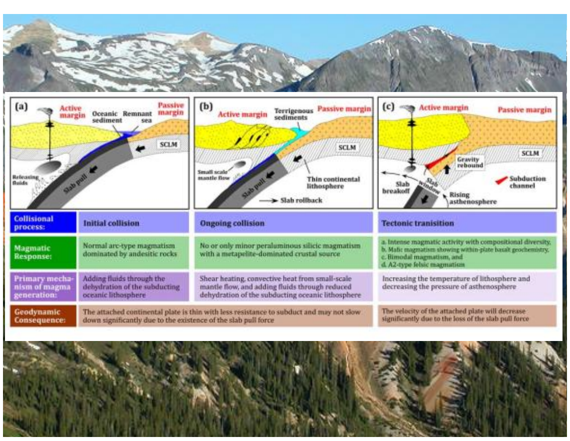

Relation between plate tectonic processes and porphyry systems:

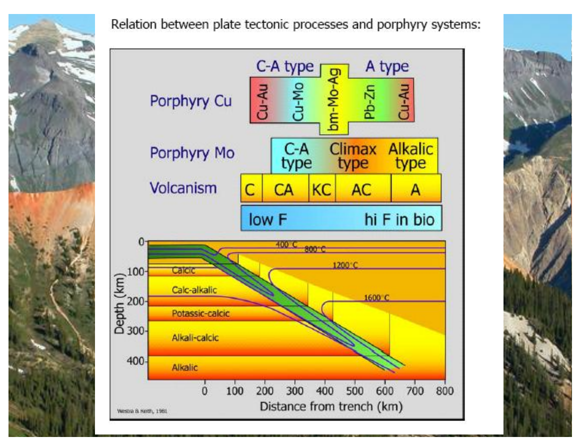

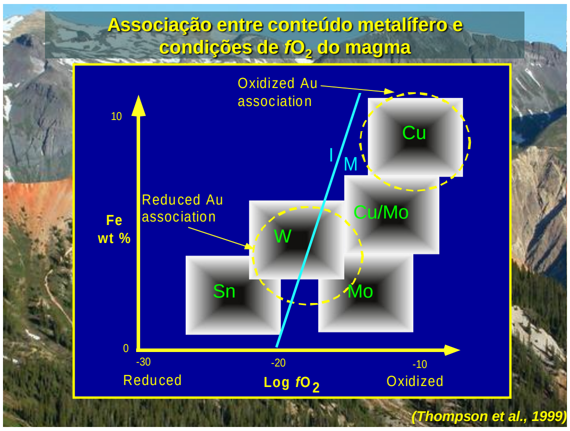

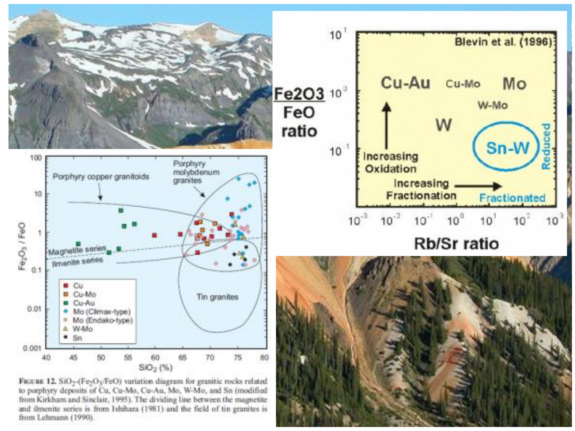

FIGURE 12. SiO_2-(Fe_2O_3/FeO) variation diagram for granitic rocks related to porphyry deposits of Cu, Cu-Mo, Cu-Au, Mo, W-Mo, and Sn (modified from Kirkham and Sinclair, 1995). The dividing line between the magnetite and ilmenite series is from Ishihara (1981) and the field of tin granites is from Lehmann (1990).

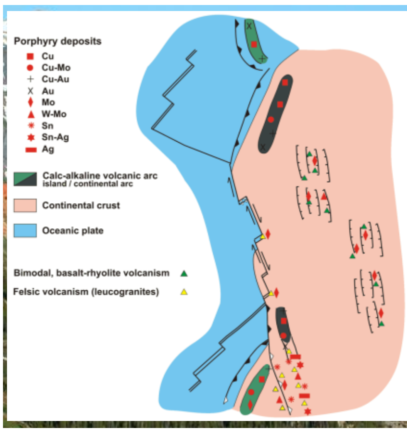

Diagrama esquemático mostrando ambientes tectônicos de ocorrência de depósitos do tipo pórfiro (Sinclair, 2006)

CARACTERÍSTICAS DOS DEPÓSITOS DE Cu-Mo PÓRFIRO (USA)

1) Associados a intrusões de quartzo monzonitos, com baixos teores de SiO_2 e de quartzo e altos teores de K_2O e Ba, ou granitos com baixos teores de sílica
2) Pórfiros de Au têm K_2O/Na_2O = 0,7 a 1,3 e os de Cu-Mo entre 0,3 e 0,7 (Bingham quartzo monzonito = 1,18, Butte = 1.35)
3) Rochas ígneas colocadas em níveis crustais rasos, de alta temperatura, fracionadas de monzonitos ou de dioritos de alto potássio
4) Estado de oxidação elevado (NNO = +2 to +3)
5) Presença de agregados e vênulas de magnetita, comumente com apatita
6) Encraves máficos com calcopirita ou sulfetos
7) Associação com rochas vulcânicas
8) Pelo menos uma rocha é porfirítica e diques de latito com estruturas de resfriamento são comuns
9) Cavidades miarolíticas com sulfetos
10) Texturas granofíricas
11) Brechas hidrotermais
12) Juntas cerradas

CARACTERÍSTICAS DOS DEPÓSITOS DO TIPO PÓRFIROS

1) Tipos de minérios: Cu-only, Cu-Mo, Cu-Mo-Au, Cu-Au, Au-only, Mo-only, W-Mo, Sn, Sn-Ag, Ag
2) Minerais de minério: calcopirita, bornita, molibdenita, cassiterita, wolframita, etc
3) Minerais de ganga: quartzo, feldspato potássico, anidrita, magnetita, biotita ± sericita ± pirita
4) Alteração hidrotermal: Potássica (biotita, magnetita, feldspato potássico, quartzo, anidrita, calcopirita), Sericítica (sericita, quartzo, pirita), Argílica intermediária (sericita, clorita, caolinita ou illita, pirita, calcita), Argílica avançada (alunita, caolinita, pirofilita, quartzo, dickita, gibbsita, pirita, enargita, covellita) e Propilítica (clorita, epidoto, albita, calcita, pirita)
5) Pelo menos dois estágios de mineralização, uma mais antiga, disseminada e/ou *stockwork* e uma tardia, em veios

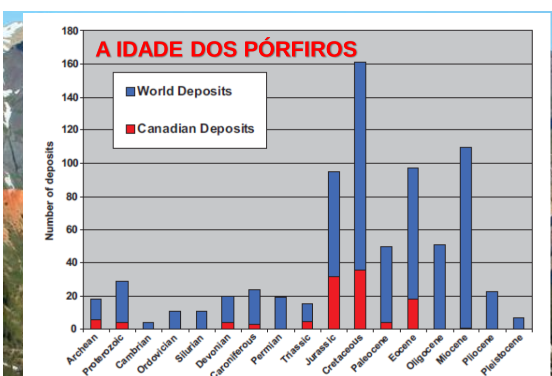

FIGURE 9. Age distribution of porphyry deposits (based on data from Kirkham and Dunne, 2000).

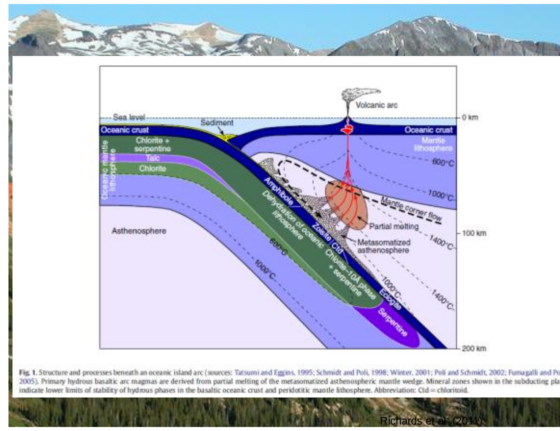

Fig. 1. Structure and processes beneath an oceanic island arc (sources: Tatsumi and Eggins, 1995; Schmidt and Poli, 1998; Winter, 2001; Poli and Schmidt, 2002; Fumagalli and Poli, 2005). Primary hydrous basaltic arc magmas are derived from partial melting of the metasomatized asthenospheric mantle wedge. Mineral zones shown in the subducting plate indicate lower limits of stability of hydrous phases in the basaltic oceanic crust and peridotitic mantle lithosphere. Abbreviation: Ctd = chloritoid.

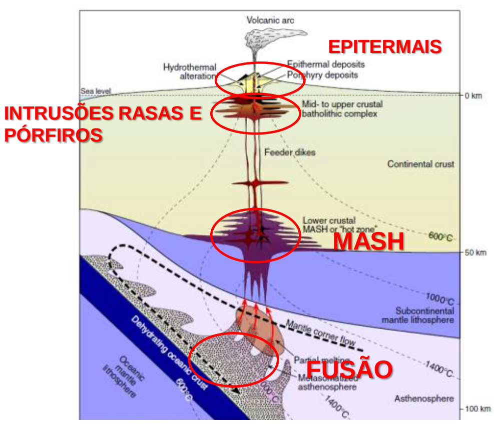

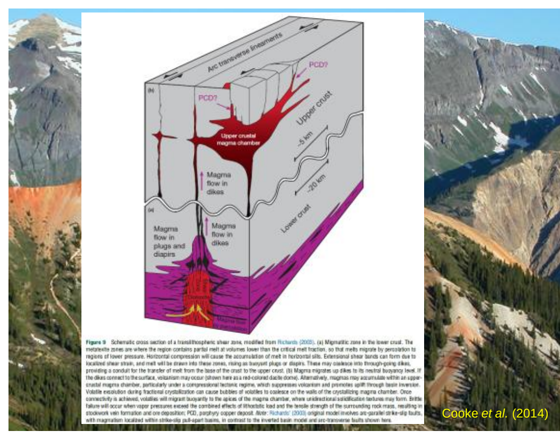

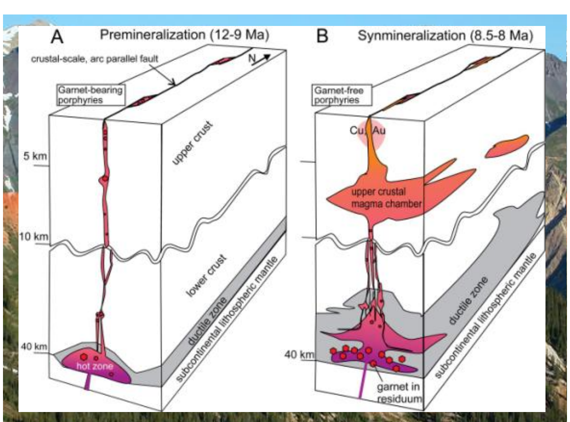

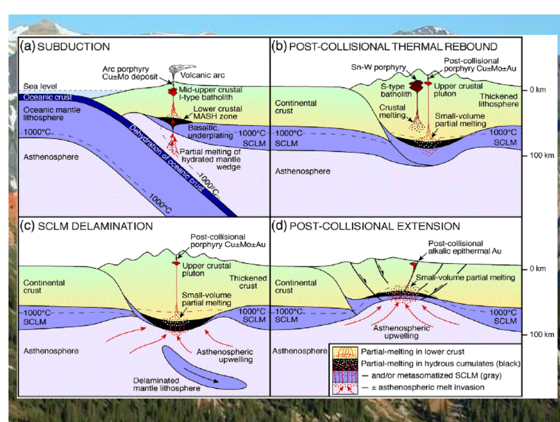

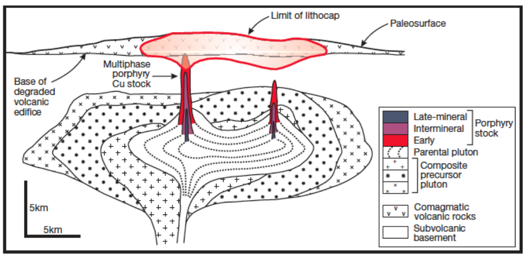

FIG. 4. Spatial relationships between porphyry Cu stocks, underlying pluton, overlying comagmatic volcanic rocks, and the lithocap. The precursor pluton is multiphase, whereas the parental pluton is shown as a single body in which the concentric dotted lines mark its progressive inward consolidation. The early, intermineral, and late-mineral phases of the porphyry Cu stocks, which span the interval during which the porphyry Cu deposits formed, originate from increasingly greater depths in the progressively crystallizing parental chamber. The volcanic sequence is a stratovolcano (but could just as readily be a dome complex; Fig. 6) and has been partly eroded prior to porphyry Cu formation. The lithocap affects the volcanic pile as well as uppermost parts of the underlying rocks. Note that subvolcanic basement rocks host much of the porphyry Cu deposit on the left, whereas that on the right is mainly enclosed by two phases of the precursor pluton. Inspired by Sillitoe (1973), Dilles (1987), Tosdal and Richards (2001), Casselman et al. (1995), and Dilles and Proffett (1995).

Depósitos do tipo pórfiro e depósitos epitermais: transição

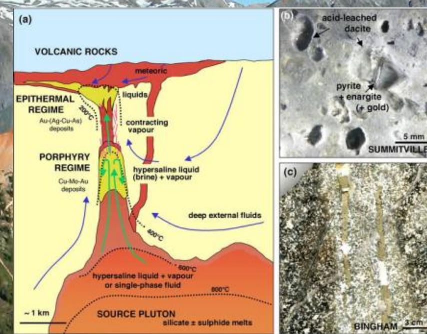

Heinrich *et al.* (2005.) Magma evolution and the formation of porphyry Cu–Au ore fluids: evidence from silicate and sulfide melt inclusions. Mineralium Deposita 39: 864 - 889

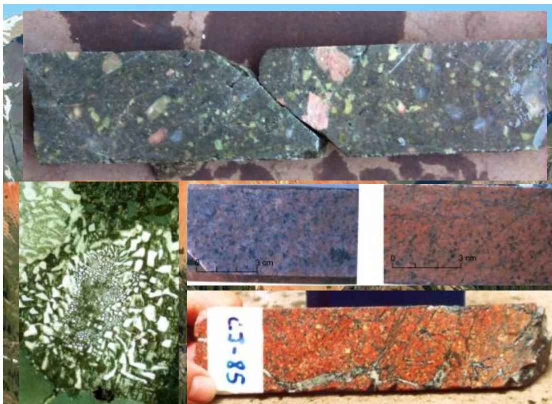

- Para formar depósitos: (1) fluido concentra-se nos setores apicais da intrusão; (2) movimento convectivo de fluidos externos ao magma; (3) fluido pode concentrar-se ao longo de estruturas ➔ permeabilidade (baixa profundidade, falhas e litotipos porosos/reativos).

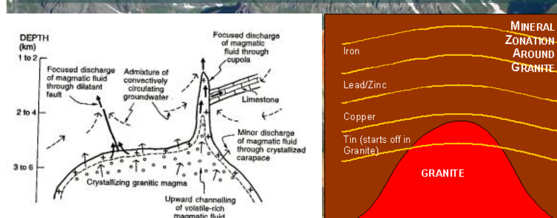

- Deposição de metais na forma de sulfetos (Cu, Mo, Pb, Ag, Bi, Sb), óxidos (Fe, Sn, W) e metais nativos (Au) ➔ decréscimo da temperatura, reação fluido-rocha, mistura de fluidos.

Depósito tipo pórfiro de Bajo de la Alumbrera, Argentina

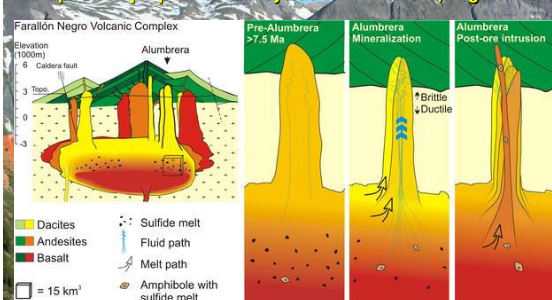

Magma evolution and the formation of porphyry Cu–Au ore fluids: evidence from silicate and sulfide melt inclusions.

Halter et al. (2005) - Mineralium Deposita, 39: 845-863.

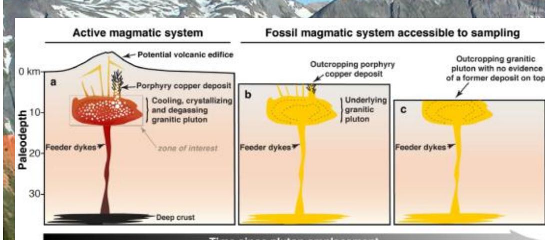

Figure 1. Architecture and temporal evolution (a to c) of a typical arc-related magmatic-hydrothermal system. The grey box in panel (a) shows that this study puts emphasis on the intrusive magmatic bodies responsible for the supply of mineralizing fluids.

Chelle-Michou et al. (2017)

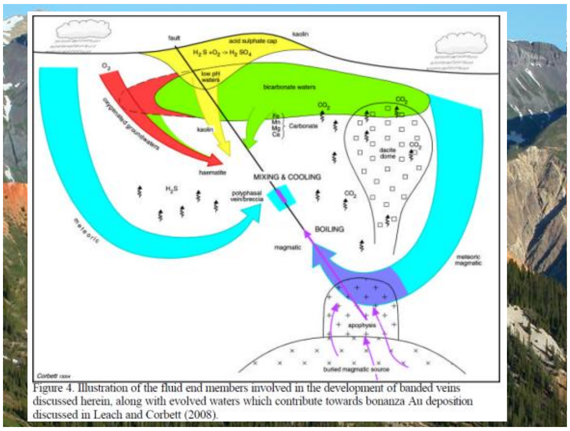
acid sulphate cap
kaolin
fault
bicarbonate waters
MIXING & COOLING
BOILING
magmatic
meteoric
Figure 4. Illustration of the fluid end members involved in the development of banded veins discussed herein, along with evolved waters which contribute towards bonanza Au deposition discussed in Leach and Corbett (2008).

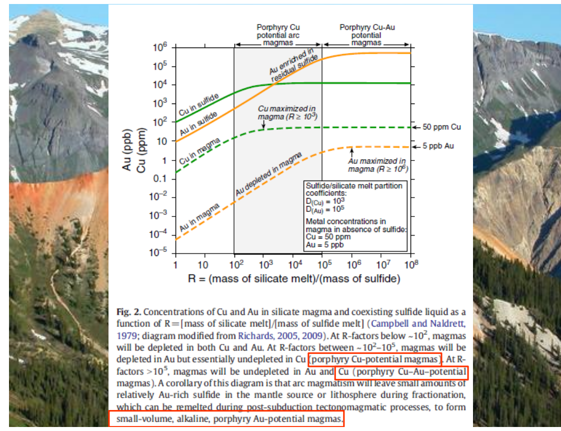
Porphyry Cu potential arc magmas
Porphyry Cu-Au potential magmas
Au (ppb)
Cu (ppm)
Cu in sulfide
Au in sulfide
Cu in magma
Au in magma
Au enriched in residual sulfide
Cu maximized in magma ($R \ge 10^3$)
Au depleted in magma
Au maximized in magma ($R \ge 10^6$)
50 ppm Cu
5 ppb Au
Sulfide/silicate melt partition coefficients:
$D_{(Cu)} = 10^3$
$D_{(Au)} = 10^5$
Metal concentrations in magma in absence of sulfide:
Cu = 50 ppm
Au = 5 ppb
R = (mass of silicate melt)/(mass of sulfide)
Fig. 2. Concentrations of Cu and Au in silicate magma and coexisting sulfide liquid as a function of R = [mass of silicate melt]/[mass of sulfide melt] (Campbell and Naldrett, 1979; diagram modified from Richards, 2005, 2009). At R-factors below ~10^2, magmas will be depleted in both Cu and Au. At R-factors between ~10^2–10^5, magmas will be depleted in Au but essentially undepleted in Cu (porphyry Cu-potential magmas). At R-factors >10^5, magmas will be undepleted in Au and Cu (porphyry Cu–Au–potential magmas). A corollary of this diagram is that arc magmatism will leave small amounts of relatively Au-rich sulfide in the mantle source or lithosphere during fractionation, which can be remelted during post-subduction tectonomagmatic processes, to form small-volume, alkaline, porphyry Au-potential magmas.

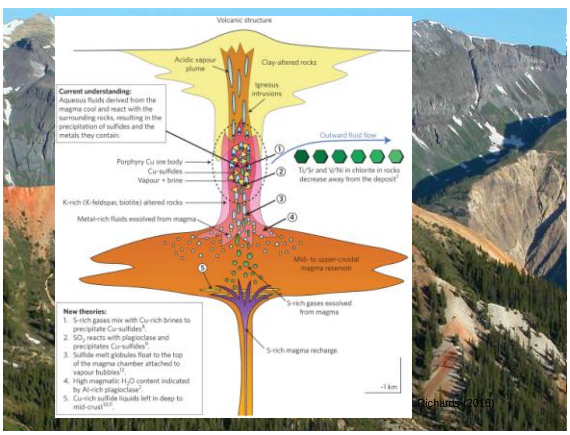
Volcanic structure
Acidic vapour plume
Clay-altered rocks
Igneous intrusions
Current understanding:
Aqueous fluids derived from the magma cool and react with the surrounding rocks, resulting in the precipitation of sulfides and the metals they contain.
Outward fluid flow
Porphyry Cu ore body
Cu-sulfides
Vapour + brine
Ti/Sr and V/Ni in chlorite in rocks decrease away from the deposit
K-rich (K-feldspar, biotite) altered rocks
Metal-rich fluids exsolved from magma
Mid- to upper-crustal magma reservoir
S-rich gases exsolved from magma
S-rich magma recharge
New theories:
Richards (2016)

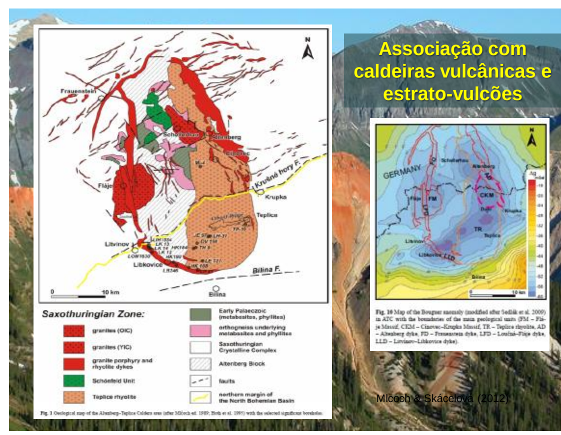
Associação com caldeiras vulcânicas e estrato-vulcões
Saxothuringian Zone:
Mlcoch & Skácelová (2012)

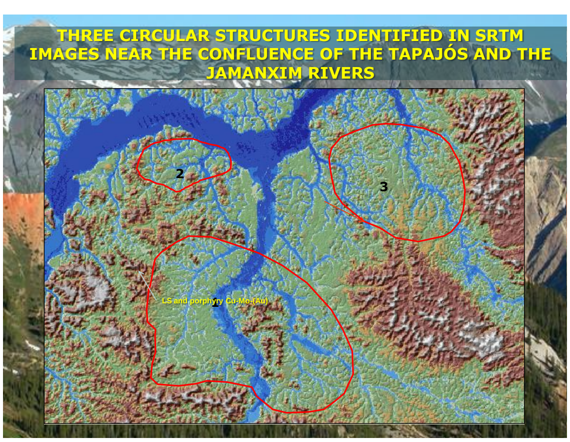
THREE CIRCULAR STRUCTURES IDENTIFIED IN SRTM IMAGES NEAR THE CONFLUENCE OF THE TAPAJÓS AND THE JAMANXIM RIVERS
2
3

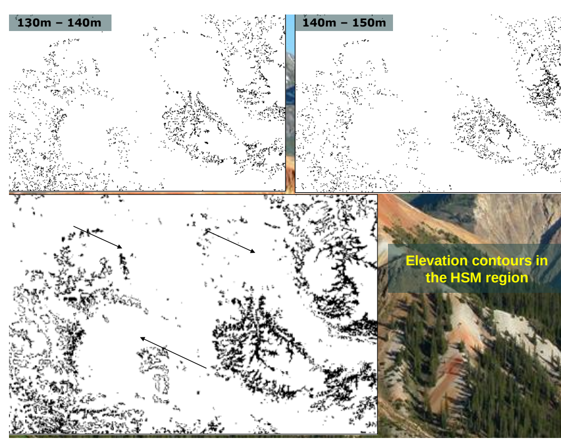
130m – 140m
140m – 150m
Elevation contours in the HSM region

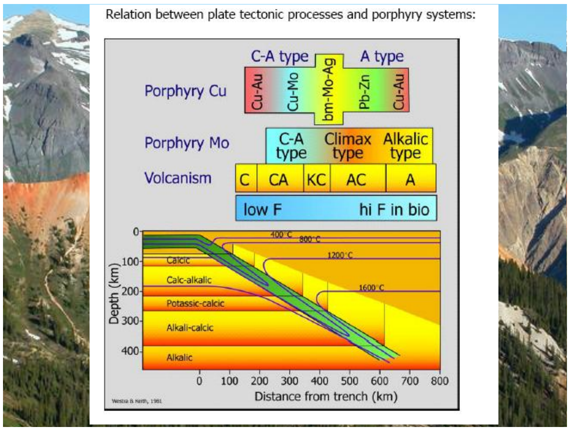
Relation between plate tectonic processes and porphyry systems:
C-A type
A type
Porphyry Cu
Cu-Au
Cu-Mo
bm-Mo-Ag
Pb-Zn
Cu-Au
Porphyry Mo
C-A type
Climax type
Alkalic type
Volcanism
C
CA
KC
AC
A
low F
hi F in bio
Calcic
Calc-alkalic
Potassic-calcic
Alkali-calcic
Alkalic
Depth (km)
Distance from trench (km)

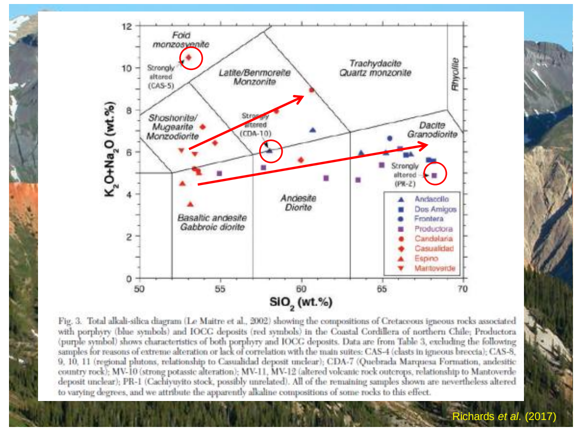
Foid monzosyenite
Strongly altered (CAS-5)
Latite/Benmoreite Monzonite
Trachydacite Quartz monzonite
Rhyolite
Shoshonite/ Mugearite Monzodiorite
Strongly altered (CDA-10)
Dacite Granodiorite
Strongly altered (PR-2)
Andesite Diorite
Basaltic andesite Gabbroic diorite
Andacollo
Dos Amigos
Frontera
Productora
Candelaria
Casualidad
Espino
Mantoverde
K_2O+Na_2O (wt.%)
SiO_2 (wt.%)
Fig. 3. Total alkali-silica diagram (Le Maitre et al., 2002) showing the compositions of Cretaceous igneous rocks associated with porphyry (blue symbols) and IOCG deposits (red symbols) in the Coastal Cordillera of northern Chile; Productora (purple symbol) shows characteristics of both porphyry and IOCG deposits. Data are from Table 3, excluding the following samples for reasons of extreme alteration or lack of correlation with the main suites: CAS-4 (clasts in igneous breccia); CAS-8, 9, 10, 11 (regional plutons, relationship to Casualidad deposit unclear); CDA-7 (Quebrada Marquesa Formation, andesitic country rock); MV-10 (strong potassic alteration); MV-11, MV-12 (altered volcanic rock outcrops, relationship to Mantoverde deposit unclear); PR-1 (Cachiyuyito stock, possibly unrelated). All of the remaining samples shown are nevertheless altered to varying degrees, and we attribute the apparently alkaline compositions of some rocks to this effect.
Richards et al. (2017)

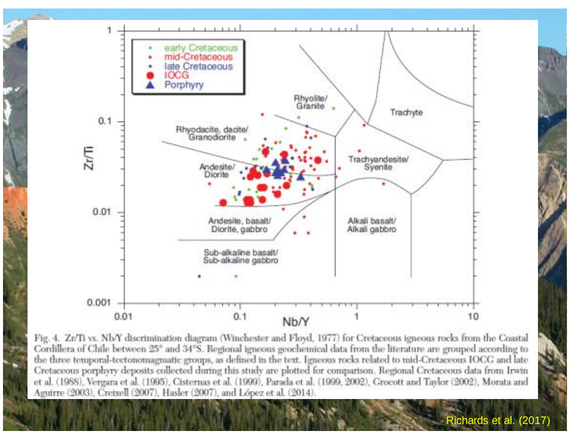
early Cretaceous
mid-Cretaceous
late Cretaceous
IOCG
Porphyry
Rhyolite/ Granite
Trachyte
Rhyodacite, dacite/ Granodiorite
Trachyandesite/ Syenite
Andesite/ Diorite
Andesite, basalt/ Diorite, gabbro
Alkali basalt/ Alkali gabbro
Sub-alkaline basalt/ Sub-alkaline gabbro
Zr/Ti
Nb/Y
Fig. 4. Zr/Ti vs. Nb/Y discrimination diagram (Winchester and Floyd, 1977) for Cretaceous igneous rocks from the Coastal Cordillera of Chile between 25° and 34°S. Regional igneous geochemical data from the literature are grouped according to the three temporal-tectonomagmatic groups, as defined in the text. Igneous rocks related to mid-Cretaceous IOCG and late Cretaceous porphyry deposits collected during this study are plotted for comparison. Regional Cretaceous data from Irwin et al. (1988), Vergara et al. (1995), Cisternas et al. (1999), Parada et al. (1999, 2002), Grocott and Taylor (2002), Morata and Aguirre (2003), Creixell (2007), Hasler (2007), and López et al. (2014).
Richards et al. (2017)

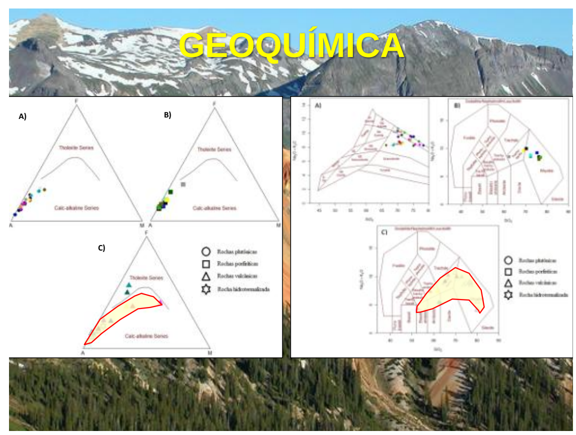
GEOQUÍMICA

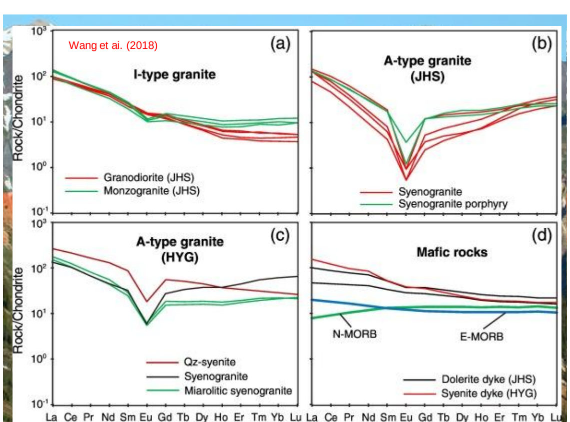
Wang et al. (2018)
(a)
I-type granite
Granodiorite (JHS)
Monzogranite (JHS)
(b)
A-type granite (JHS)
Syenogranite
Syenogranite porphyry
(c)
A-type granite (HYG)
Qz-syenite
Syenogranite
Miarolitic syenogranite
(d)
Mafic rocks
N-MORB
E-MORB
Dolerite dyke (JHS)
Syenite dyke (HYG)
Rock/Chondrite
La Ce Pr Nd Sm Eu Gd Tb Dy Ho Er Tm Yb Lu

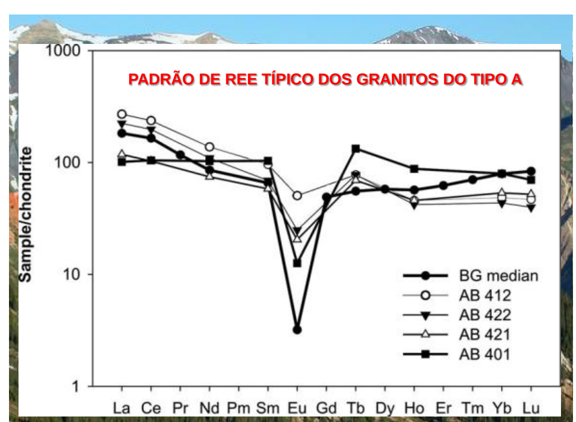
PADRÃO DE REE TÍPICO DOS GRANITOS DO TIPO A
Sample/chondrite
BG median
AB 412
AB 422
AB 421
AB 401
La Ce Pr Nd Pm Sm Eu Gd Tb Dy Ho Er Tm Yb Lu

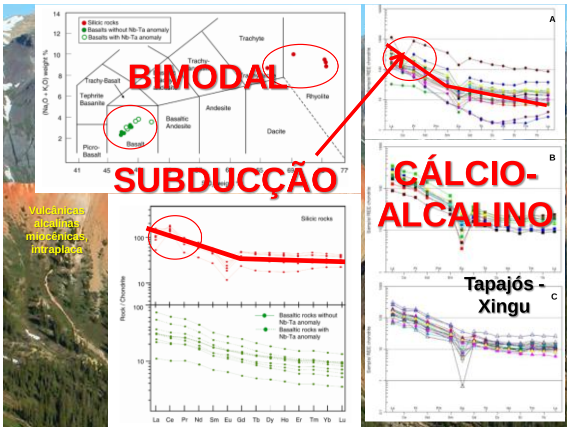

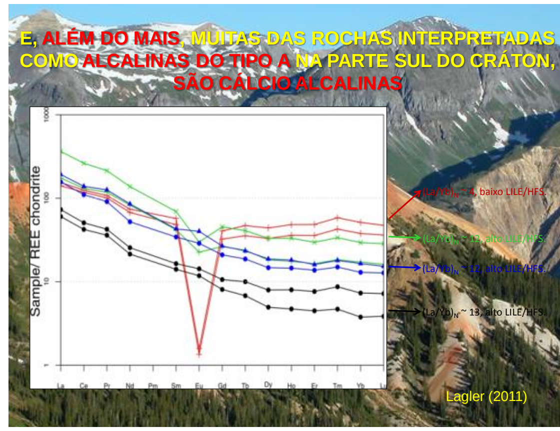

MAGMAS EM ARCOS MAGMÁTICOS

1) Tipicamente cálcio-alcalinos
2) Se associam a zonas de subducção
3) Magmas oxidados (formação de mineralizações *high-sulfidation*)
4) Alto conteúdo de cloro
5) Séries magmáticas estendidas (basaltos, andesitos, dacitos, riodacitos e riolitos
6) Variável conteúdo de potássio (fracionamento e contaminação)
7) Também ocorrem associados a sagducção no arqueano, mas geralmente essas rochas estão associadas com sanukitóides, o que sugere subdução

MAGMATISMO INTRA-PLACA

1) Tipicamente alcalinos
2) Tipicamente bi-modal (basaltos e riolitos)
3) Magmas reduzidos (formação de mineralizações *low-sulfidation*)
4) Alto conteúdo de flúor

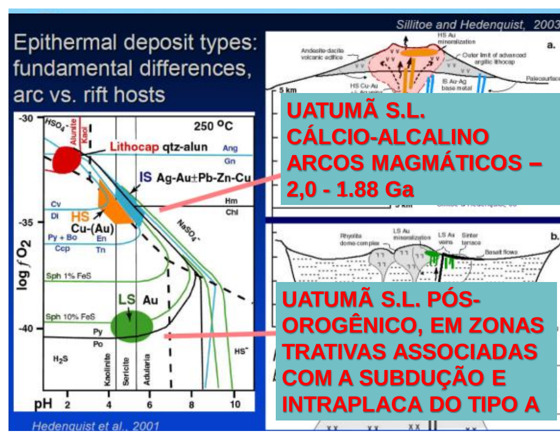

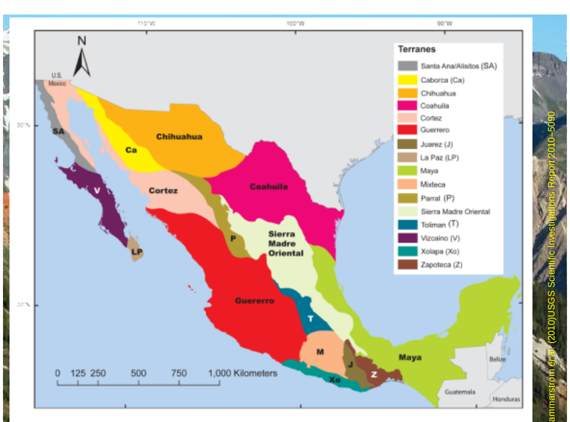

Figure 2. Simplified tectonostratigraphic terrane map of Mexico, based on Coney and Campa (1987).

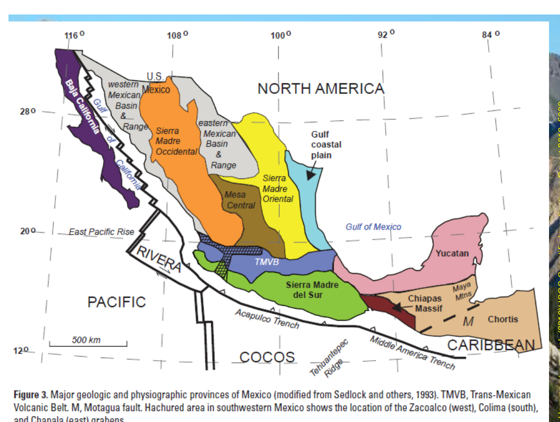

Figure 3. Major geologic and physiographic provinces of Mexico (modified from Sedlock and others, 1993). TMVB, Trans-Mexican Volcanic Belt. M, Motagua fault. Hachured area in southwestern Mexico shows the location of the Zacoalco (west), Colima (south), and Chapala (east) grabens.

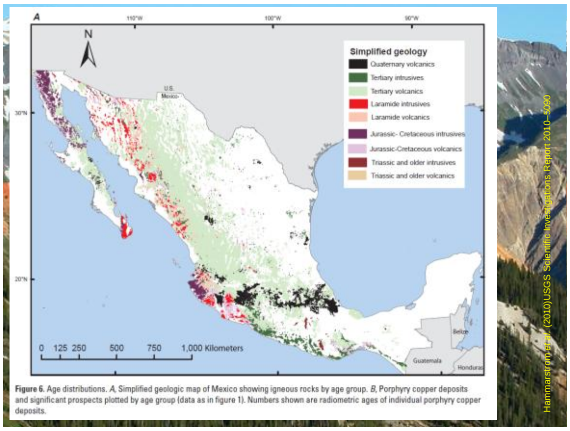
A
Simplified geology
Quaternary volcanics
Tertiary intrusives
Tertiary volcanics
Laramide intrusives
Laramide volcanics
Jurassic- Cretaceous intrusives
Jurassic-Cretaceous volcanics
Triassic and older intrusives
Triassic and older volcanics
0 125 250 500 750 1,000 Kilometers
Figure 6. Age distributions. A, Simplified geologic map of Mexico showing igneous rocks by age group. B, Porphyry copper deposits and significant prospects plotted by age group (data as in figure 1). Numbers shown are radiometric ages of individual porphyry copper deposits.
Hammarstrom et al. (2010)USGS Scientific Investigations Report 2010–5090

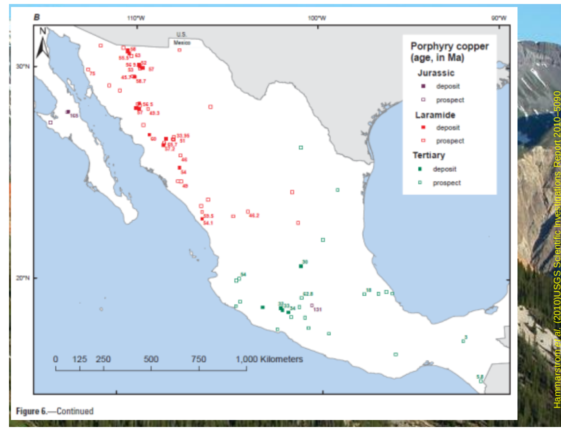
B
Porphyry copper (age, in Ma)
Jurassic
deposit
prospect
Laramide
deposit
prospect
Tertiary
deposit
prospect
0 125 250 500 750 1,000 Kilometers
Figure 6.—Continued
Hammarstrom et al. (2010)USGS Scientific Investigations Report 2010–5090


FINAL DA AULA 5